The AASHTO Guide Specification for Alternate Load-factor Design Procedures for Steel Beam Bridges

MICHAEL A. GRUBB

The 13th Edition of the AASHTO *Standard Specifications for Highway Bridges*[1] includes provisions for Load Factor Design (LFD) of steel bridges by the strength design method. Limit-state criteria are provided in LFD that ensure that specified structural performance requirements are satisfied.[2] In LFD, shear and moment envelopes are determined by elastic analysis with limited distribution for the effects of local yielding. Therefore, sections are proportioned for strength equal to or greater than required by the envelopes.

After 10 years of AISI-sponsored research, Autostress-design procedures are now included in the AASHTO *Guide Specification for Alternate Load-Factor Design Procedures for Steel Beam Bridges Using Braced Compact Sections*.[3] Autostress is a procedure that extends the existing LFD rules by introducing improved limit-state criteria. These criteria permit inelastic load redistribution in continuous-beam bridges under heavy loads while satisfying the same structural performance requirements as LFD.[4]

Design specifications have long recognized the reserve strength of steel members beyond the first-yield stress. For instance, LFD permits a 10% redistribution of the peak moments at intermediate supports to maximum positive moment sections for compact continuous beams at higher loads. The Autostress procedures can be viewed as a refinement of this 10% redistribution allowance to more closely approximate actual behavior. The ability of continuous steel members to adjust automatically for the effects of local yielding is recognized. Elastic negative bending moments at higher loads are automatically redistributed by the structure to positive bending regions. To emphasize this redistribution occurs automatically, the term Autostress has been used for the suggested procedures based on the new criteria. Taking advantage of this inherent ability permits a designer to use prismatic steel members in continuous spans along the entire bridge length, or in between field splices. The resulting benefits include lower fabrication costs, and elimination of structural details with undesirable fatigue characteristics. For instance, cover plates can be eliminated from rolled beams. Similarly, flanges of welded sections with similar proportions will have fewer splices and thickness changes.

The development of most of the guide specification provisions was based on test results for several component specimens with proportions similar to rolled beams.[5] Other provisions were based on research to support the Proposed AISC Load and Resistance Factor Design (LRFD) building-design specification.[6] The research suggests that well-established principles of plastic design can be extended to compute the resistance at Maximum Load by mechanism formation. Also, structural performance requirements at Overload can be satisfied by establishing camber requirements to offset the effects of local yielding in addition to the elastic dead-load deflections. Because the mechanism resistance generally is high, permanent deflection (Overload) criteria rather than strength (Maximum Load) criteria usually govern. This results in more economical steel beam bridge designs. The Autostress procedures were first applied and confirmed in the design and testing of an in-service rolled-beam bridge—the Whitechuck River Bridge in the Mt. Baker National Forest near Darrington, Wash.[7]

This paper contrasts present LFD with the Autostress procedures, and briefly summarizes the background research that led to the development of the guide specification provisions. Thus, it also serves as an in-depth commentary to the specification. The guide specification is presently

Michael A. Grubb is Assistant Manager, Bridge Engineering, AISC Marketing, Inc., Pittsburgh, Pennsylvania.

Table 1. Structural Performance Requirements

Load Level	Structural Performance Requirement
Service load $[D + (L + I)]$ (nominal dead load plus standard vehicles plus impact)	Provide adequate fatigue life, limit concrete cracking and live-load deflections
Overload $[D + (5/3*(L + I))]$ (nominal dead load plus occasional heavy vehicles plus impact)	Limit permanent deformations that otherwise could create objectionable riding quality
Maximum load $1.3*[D + (5/3*(L + I))]$ (limited occurrences of load factor times Overload)	Provide load resistance equal to or greater than maximum load

limited to rolled-beam bridges and similar welded-beam bridges of equivalent dimensions that are adequately braced. Research is now in progress to extend the Autostress procedures to slender plate-girder sections.[8]

LOADS AND PERFORMANCE REQUIREMENTS

Members designed by the LFD method of AASHTO[1] are proportioned for multiples of the design loads. They are required to meet specified structural performance requirements for three theoretical load levels—Service Load, Overload and Maximum Load. It is important to distinguish between the three load levels. Table 1 lists the load levels in order of increasing load. The second column of Table 1 lists the structural performance requirement for each load level, which is a brief verbal description of the performance required of a bridge at that load level. The guide specification requires that members be proportioned to meet the same LFD structural performance requirements at the same three load levels.

Service Load

Service Load is the same load as that used in AASHTO working stress design. The limit-state criteria at Service Load ensure that the fatigue life and live-load deflection of a member are controlled within acceptable limits. The guide specification invokes the same limit-state criteria as LFD to satisfy fatigue and live-load requirements. Stress ranges are kept within allowable fatigue limits and elastic live-load deflections are treated in accordance with current practice. Furthermore, the guide specification requires that concrete cracking be controlled by invoking the current AASHTO rules (Sect. 8.16.8.4) for distribution of flexural reinforcement.[5] Control of slab cracking is a significant requirement to ensure overall high quality construction.

Overload

The structural performance requirement at overload is also concerned with durability of the structure. Permanent deformations, caused by occasional heavy vehicles, that could be objectionable to the riding quality of the structure must be controlled. In LFD, permanent deformations are controlled by limiting Overload flange stresses to $0.80*F_y$ (non-composite sections) or $0.95*F_y$ (composite sections) in positive and negative bending. F_y is the yield strength of the steel section. For compact sections, 10% of the negative interior-pier moments may be redistributed to maximum positive moment sections before computing the stresses.

The Autostress procedures in the guide specification place no limit on the stress in negative bending at Overload. Instead, a continuous-span bridge is allowed to undergo controlled plastic deformations at interior piers that will stabilize after a few cycles of an overload vehicle. These plastic deformations normally occur only in the flange outer fibers—they do not create a plastic hinge. Instead, they result in the formation of automoments, so-called because they form automatically. The automoments are residual moments that, along with the dead load, remain in the structure after the Overload is removed. The automoments ensure that the structure will behave elastically to all subsequent loads not exceeding the Overload. Thus, the stress at the pier sections need not be restricted. The only limit-state criterion for negative bending at Overload in the guide specification is that the rebars over the piers remain elastic to help ensure that any concrete cracks will close when the Overload is removed. Also, it is suggested the rebars be distributed as mentioned earlier.

In positive bending, the guide specification retains the current LFD Overload limit-state criteria. The stress in positive bending due to the elastic Overload moments plus the automoments is limited to $0.95*F_y$ for composite sections and $0.80*F_y$ for non-composite sections. This limit is retained to help control any permanent deflections caused by positive bending. Thus, the automoments are simply a refinement of the 10% redistribution allowed in LFD. They reduce the elastic pier moments and increase proportionately the maximum positive moments.

The automoment computations are based on actual moment-rotation behavior of the interior-pier sections. Typical moment-rotation curves are included in the guide specification to aid in the automoment computations if experimental curves are not available. Permanent deflections caused by the automoments are also calculated and included in the dead-load camber. If no Overload occurs during the life of the structure, some of the automoment camber would remain. However, this would not be objectionable because the automoment camber is usually comparable to the composite dead-load camber which is relatively small. The formation and computation of automoments will be discussed later in more detail.

Maximum Load

The Maximum load structural performance requirement deals primarily with load resistance; the criterion is that the Maximum load must be able to cross the bridge a limited

number of times. In LFD, this is achieved for compact sections by limiting the elastic Maximum load moment at any section to be below the plastic moment. The plastic moment is equal to the yield strength, F_y, times the plastic section modulus, Z (values of Z for rolled sections are given in Ref. 9). Also, for compact sections, 10 percent of the peak negative moments may be redistributed before the comparison is made, as previously discussed for Overload.

The AISC building design specification,[9] LFD, and the guide specification each have slightly different criteria to qualify a section as compact, which can lead to confusion. For the remainder of this paper and in the guide specification, a compact section is defined as a section that can both reach the plastic moment and rotate inelastically at the plastic moment a limited amount. In the guide specification, the Maximum load performance requirement is achieved from the condition that the plastic mechanism strength equals or exceeds the fully factored load. The resistance of continuous bridge members can be determined by the plastic-design concept of mechanism analysis if the section is compact with adequate inelastic rotation capacity, and if the nominal yield strength of the steel does not exceed 50,000 psi. This recognized the fact that plastic redistribution takes place in continuous beams with braced compact sections at maximum load.

In a continuous bridge, the first plastic hinges normally form at the piers. Thus, conventional plastic design, as defined in Part 2 of the AISC building design specification, requires that the pier sections be able to reach the plastic moment, and that the hinges at the piers be able to rotate inelastically at the plastic moment as the load redistributes to the maximum positive moment sections. For such behavior, the AISC Part 2 specification requires that the flange- and web-slenderness ratios must be within specified limits, the lateral bracing of the compression flange must be adequate, and the pier shears must be less than or equal to the plastic shear force.

Compact sections with flange- and web-slenderness ratios in the upper range of the specified slenderness limits in the guide specification are able to reach the plastic moment, but may not have enough available inelastic rotation capacity at the plastic moment. Rather than specify more stringent requirements limiting the number of sections that can be used, the guide specification requires that an effective plastic moment[10] be determined for the pier sections in the strength analysis at Maximum load. The effective plastic moment is a reduced moment, based on the actual section geometry, at which the pier sections can be considered to have adequate rotation capacity. For compact sections with flange- and web-slenderness ratios in the lower range of the specified slenderness limits, the effective plastic moment will equal the plastic moment. The effective plastic moment will be discussed in more detail in the next section.

For compact sections in positive bending, the maximum strength at maximum load according to the guide specification is computed assuming a fully plastic stress distribution in the sections, including the concrete slab. The moment capacity then equals the sum of the moments about the plastic neutral axis of the composite section of all compressive and tensile forces. The guide specification also states that whenever a composite section in positive bending reaches this plastic moment, no further plastic rotation is permitted. Thus, if the first hinge should form in positive bending, the limit state is reached. This is because there has been little research on the available rotation capacity of composite sections in positive bending.

REVIEW OF RESEARCH STUDIES

Maximum Load

Consider a two-span continuous beam loaded by a uniform dead load, $1.3D$, and by the AASHTO HS20 Maximum load lane load plus impact, $1.3[5/3(L + I)]$, as shown in Fig. 1. The moment $M-$ represents the interior-pier moment, and the moment, $M+$, represents the maximum positive moment. Because yielding is expected at Maximum load, the permanent deflections that would remain in the structure after the live load is removed are shown. The inelastic rotation at the pier is $\theta P-$. The permanent rotation at the maximum positive moment section, caused by yielding in positive bending, is $\theta P+$ (not shown in Fig. 1).

Figure 2 shows the basic design procedure in LFD at

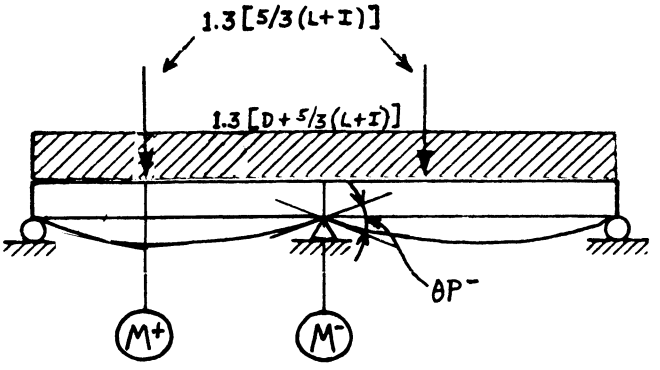

Fig. 1. Two-span continuous beam at maximum load

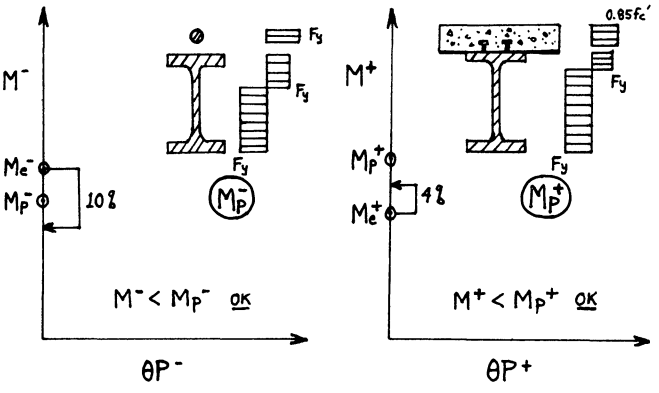

Fig. 2. Moment vs. permanent rotation-load factor design

maximum load. Two graphs are shown; $M-$ vs. $\theta P-$, and $M+$ vs. $\theta P+$. The elastic Maximum Load moments at the interior pier, M_e-, and at the maximum positive moment section, M_e+, are plotted on the ordinates of the respective graphs ($\theta P- = \theta P+ = 0.$). Also plotted is the plastic moment in negative bending, M_p-, and the plastic moment in positive bending, M_p+. M_p- is computed assuming that the concrete slab does not carry any tensile stresses, and that the slab reinforcement is composite with the steel beam. This is allowed if the reinforcement and slab are continuous over the interior support. M_p+ is computed including the concrete slab, and consequently, is usually a larger value. In LFD, it can be interpreted that all sections are elastic up to the plastic moment. If the pier section meets specified slenderness and lateral-bracing requirements, LFD allows M_e- to be reduced by 10%, as shown in Fig. 2. This reduction in moment must be redistributed to the maximum positive moment section. In this particular case, M_e+ is increased by 4% of M_e-. Since the total moments after redistribution are everywhere less than M_p- and M_p+, the design is satisfactory at maximum load.

In conventional plastic design, the interior-pier section is assumed to be elastic up to M_p-, then to rotate inelastically at M_p- as shown in Fig. 3. Also shown in Fig. 3 is a moment-rotation curve that is typical of the actual behavior of a compact section. Residual stresses result in some yielding of the section before reaching M_p-. The section may then be able to exceed M_p- because of strain hardening before eventually unloading due to local buckling of the web and compression flange. M_p- is thus a moment that provides a convenient computational device, but has no specific relation to actual behavior. The design assumption of rotating at M_p- is satisfied as long as $M-$ is greater than or equal to M_p- during inelastic rotation, which could include the unloading portion.

Since the interior-pier section is assumed to rotate at a constant M_p-, the maximum moment in positive bending $M+$ can be easily computed from the statics of a simple beam with an end moment equal to M_p-, as illustrated in Fig. 3. If the computed $M+$ is less than M_p+, a mechanism

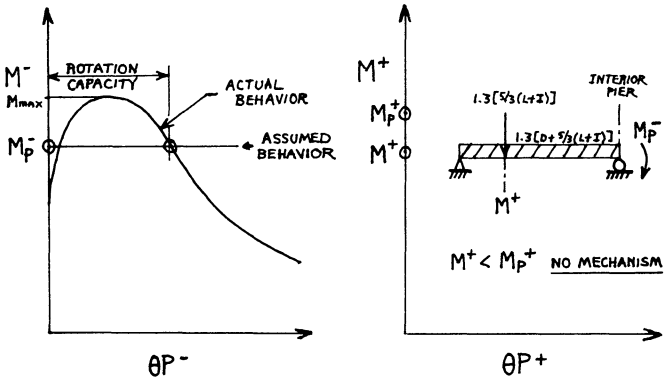

Fig. 3. Moment vs. permanent rotation-plastic design

does not form and the design is satisfactory. It is assumed that the positive bending section is also elastic up to M_p+ ($\theta P+ = 0$). To make the simplifying assumption of elastic-perfectly-plastic behavior, it must be assumed that the pier section has adequate inelastic rotation capacity at M_p- until the positive moment section reaches M_p+. The rotation capacity is defined as the plastic rotation at the point on the downward portion of the actual curve where the moment equals M_p- (Fig. 3). Criteria are needed to ensure that a section has adequate rotation capacity in order to use plastic-design assumptions.

For adequate rotation capacity at the plastic moment at each rotating hinge, the plastic-design procedures in Part 2 of the AISC Specification[9] require the slenderness ratio of the compression flange meet the limit

$$\frac{b'}{t} \leq \frac{1{,}565}{\sqrt{F_{yf}}} \tag{1}$$

where b' is the width of the projecting flange element, t is the flange thickness, and F_{yf} is the yield strength of the compression flange in psi. The web slenderness should meet

$$\frac{D}{t_w} \leq \frac{12{,}377}{\sqrt{F_{yf}}} \tag{2}$$

F_{yf} is used for the web because plastic web buckling is governed by flange strain. D is the distance between flanges and t_w is the web thickness. It is assumed in Eq. 2 that D represents 95% of the total depth of the section d. The above flange and web limits are 7.0 and 55.4, respectively, for 50,000 psi steel.

The web slenderness requirement in Eq. 2 applies to symmetrical sections. Figure 4 shows the cross section at an interior pier of a continuous bridge. When the section is subjected to negative bending, the reinforcing steel is often assumed to act compositely with the beam so the neutral axis shifts toward the slab. Yielding further shifts the neutral axis. This increase of the depth of the web in compression is illustrated for the unsymmetrical steel test specimen 188-3-6 from Ref. 11 in Fig. 5. This increased depth of the web in compression was determined to have an important effect on the rotation capacity of unsymmetrical sections.[12] Thus, the guide specification states that for unsymmetrical sections, where the distance from the neutral axis to the compression flange exceeds $D/2$, the web requirement in Eq. 2 must be modified by replacing D with the quantity $2D_{cp}$. D_{cp} is the distance to the compression flange from the neutral axis at the plastic moment.

To use plastic-design assumptions, the guide specification presently states that steels with a nominal yield strength less than or equal to 50,000 psi must be used. The section at the hinge must also be able to reach the plastic moment. The Proposed AISC LRFD Specification[6] gives requirements for a section that can reach the plastic moment with limited rotation capacity at the plastic moment. These requirements were adopted in the guide specifica-

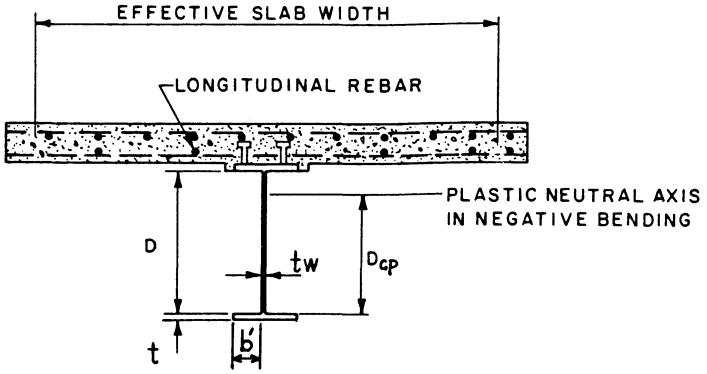

Fig. 4. Cross section at interior pier

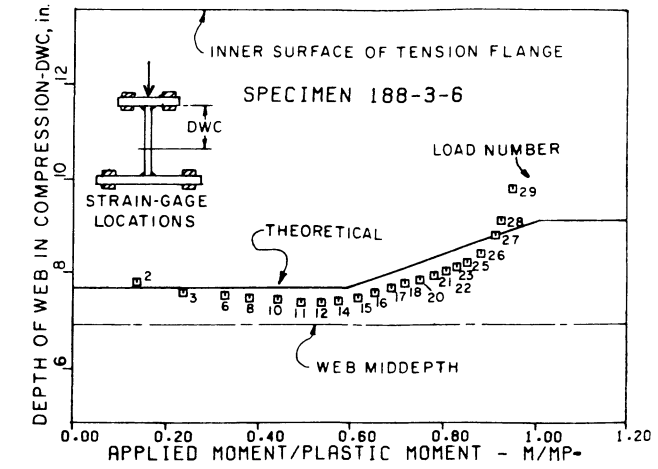

Fig. 5. Static neutral-axis location for specimen 188 3-6

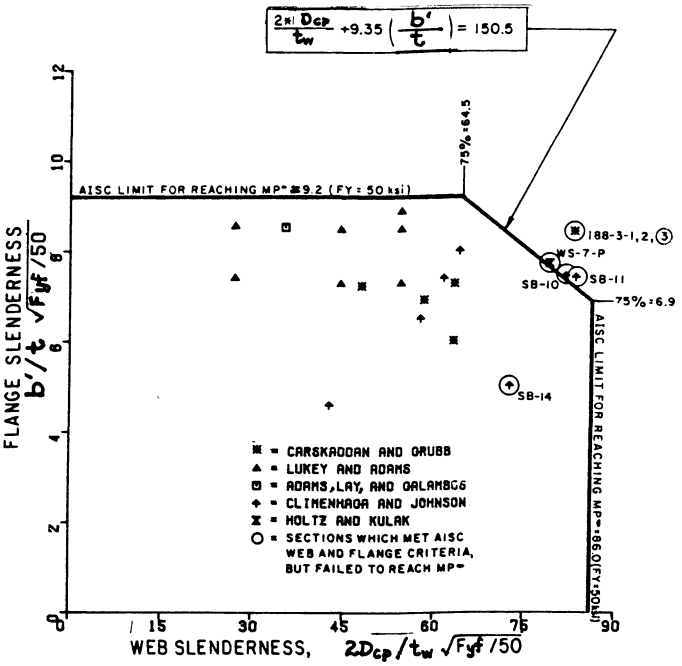

Fig. 6. Flange-web slenderness interaction diagram to just reach M_p

tion. To qualify, the slenderness ratio of the projecting compression-flange element must meet

$$\frac{b'}{t} \leq \frac{2{,}055}{\sqrt{F_{yf}}} \tag{3}$$

The web slenderness must meet

$$\frac{D}{t_w} \leq \frac{19{,}230}{\sqrt{F_{yf}}} \tag{4}$$

These are simply the requirements adopted from Part 1 of the AISC Specification[9] with F_{yf} expressed in units of psi rather than ksi. Also, it is assumed D corresponds to 95% of the total depth. Again, D should be replaced by $2D_{cp}$ for unsymmetrical sections in negative bending. The above flange and web limits are 9.2 and 86.0, respectively, for 50,000 psi steel.

A review of the data available in the literature plotted in Fig. 6 suggests the section may not be able to reach the plastic moment when the flange and web slenderness ratios both exceed 75 percent of the limits in Eqs. 3 & 4. The following interaction equation[11] is given in the guide specification to redefine the allowable limits when this occurs

$$\frac{D}{t_w} + 9.35\left(\frac{b'}{t}\right) \leq \frac{33{,}650}{\sqrt{F_{yf}}} \tag{5}$$

Once again, D should be replaced by $2D_{cp}$ if the distance from the neutral axis to the compression flange exceeds $D/2$.

For compact sections, the guide specification also requires that the shear force at rotating hinges be less than the plastic shear force

$$V \leq 0.55^* F_y^* d^* t_w \tag{6}$$

The total depth of the section d is used in Eq. 6.

Finally, lateral bracing of the compression flange adjacent to a rotating hinge is also an important consideration. The bracing helps to prevent lateral buckling of the flange, which has a detrimental effect on rotation capacity. The lateral bracing requirements in the guide specification are adopted directly from the Proposed AISC LRFD Specification.[6] The limit for the required lateral bracing is given as

$$\frac{L_b}{r_y} \leq \frac{[3.6 - 2.2(M_1/M_2)] * 10^6}{F_y} \tag{7}$$

L_b is the distance between points of bracing of the compression flange; r_y is the radius of gyration of the steel beam with respect to the Y-Y axis; F_y is the yield strength in psi, and M_1 and M_2 are the moments at the two adjacent brace points. M_1/M_2 is positive for a member bent in single curvature. For bracing adjacent to the interior pier, M_2 is equal to the effective plastic moment $M_{pe}-$, for compact sections. A trial-and-error procedure is required to determine L_b. The existing LFD lateral bracing requirement in Article 10.48.2.1(c) need not be considered because it is

limited to conditions of constant moment and St. Venant torsional resistance only. Also, bearing stiffeners are required at rotating hinge locations.

To determine the available rotation capacity at the AISC Part 2 slenderness limits (Eqs. 1 and 2), an unsymmetrical steel beam with proportions approximating these limits was tested (specimen 188-3-6 from Ref. 11). The specific slenderness ratios of the specimen were $b'/t = 6.69$ and $2D_{cp}/t_w = 56.2$. The moment vs. permanent rotation curve for the specimen is plotted in Fig. 7. The available rotation capacity at the plastic moment was computed to be 58.0 mrads (1 mrad equals .001 radian, or a slope of approximately ⅛ inch in 10 feet).

Sections with compression-flange slenderness ratios between 7.0 and 9.2, and web-slenderness ratios between 55.4 and 86.0 (assuming 50,000 psi steel) may not have 58.0 mrads of inelastic rotation capacity at the plastic moment. Consequently, the guide specification requires that an effective plastic moment, $M_{pe}-$, be used at the pier sections in the mechanism analysis at maximum load. $M_{pe}-$ is a reduced moment that accounts for the effects of local web and flange buckling and is computed as

$$M_{pe}- = R_f M_{pf}- + R_w M_{pw}- \quad (8)$$

$M_{pf}-$ is the flange component of the plastic moment, including the composite rebars. $M_{pw}-$ is the web component of the plastic moment. R_f and R_w are reduction factors for the web and flange, respectively.

The reduction factors R_f and R_w are computed from effective yield strengths of the compression flange and web. The effective yield strength of the compression flange F_{yfe} is computed by rearranging and non-dimensionalizing Eq. 1

$$F_{yfe} = 0.0845 * E\left(\frac{t}{b'}\right)^2 \leq F_{yf} \quad (9)$$

E is Young's modulus. Substituting $2D_{cp}$ for D, then rearranging and non-dimensionalizing Equation 2 gives the effective yield strength of the web as

$$F_{ywe} = 1.32 * E\left(\frac{t_w}{D_{cp}}\right)^2 \leq F_{yf} \quad (10)$$

F_{ywe} is limited to F_{yf} because again, plastic web buckling is governed by flange strain. The reduction factors are then simply computed as $R_f = F_{yfe}/F_{yf}$ and $R_w = F_{ywe}/F_{yf}$. For sections with compression-flange slenderness ratios meeting Equation 1, and web-slenderness ratios meeting Equation 2, $M_{pe}-$ equals M_p-. Thus, in the mechanism analysis at maximum load $M+$ is determined as illustrated in Fig. 3 except that $M_{pe}-$ is substituted for M_p- at the pier section. Like M_p-, $M_{pe}-$ is a computational device that gives good results.

To validate this concept, moment-rotation test results published by several investigators[11-18] were examined. The data, presented in Table 2, represent unsymmetrical and symmetrical steel sections and composite steel-concrete

Table 2. Moment-rotation Test Data

Ref. No.	Test Specimen	$\frac{b'}{t}$	$\frac{2D_{cp}}{t_w}$	M_p, k/ft	$\frac{M_{max}}{M_p-}$	$\frac{M_{pe}-}{M_p-}$	$\theta P-$, mrads
11	188-3-6(A)	6.69	56.2	268.1	1.15	0.974	63.3
	188-3-5(A)	6.99	46.2	209.3	1.31	0.950	168.1
U	188-3-7(A)	5.80	60.9	277.5	1.10	0.929	63.9
	188-3-8(A)	7.04	61.1	312.6	1.08	0.879	71.2
12	188-3-1(A)	8.02	78.7	274.1	1.08	0.623	71.5
	188-3-2(A)	8.02	78.7	274.1	1.01	0.623	87.4
U	188-3-3(A)	8.02	78.7	274.1	0.98	0.623	58.5
13	*188-3-4E (A)	8.02	96.6	319.6	0.89	0.574	135.0
U	*188-3-4W(A)	8.02	96.6	319.6	0.89	0.574	110.0
14	HT-28(B)	7.87	32.6	56.4	1.14	0.777	157.3
	HT-43(B)	7.87	32.6	56.4	1.13	0.777	80.0
S	HT-52(C)	7.87	32.6	56.4	1.14	0.777	309.3
15	A-1(B)	9.42	29.9	133.4	1.36	0.725	325.1
	A-2(B)	8.15	29.9	118.5	1.40	0.909	296.4
S	B-1(C)	9.71	42.7	40.7	1.12	0.629	103.0
	B-2(B)	7.00	42.7	32.6	1.17	0.952	138.6
	B-3(B)	8.15	42.7	36.1	1.14	0.785	157.8
	B-4(B)	8.89	42.7	38.3	1.06	0.703	213.0
	B-5(B)	9.16	42.7	39.1	1.04	0.677	172.8
	C-1(B)	9.69	52.2	53.3	1.13	0.649	111.2
	C-2(B)	7.00	52.2	43.3	1.25	0.953	110.7
	C-3(B)	8.16	52.2	47.6	1.16	0.795	120.7
	C-4(B)	8.89	52.2	50.3	1.13	0.719	93.6
	C-5(B)	8.55	52.2	49.1	1.14	0.752	141.8
16	WS-1(D)	9.67	76.3	307.1	1.02	0.561	252.1
	WS-2(C)	9.67	95.7	410.1	0.98	0.490	118.4
S	WS-3(D)	9.67	115.3	524.6	0.89	0.439	161.4
	WS-4(D)	9.67	137.8	645.4	0.86	0.398	166.2
	WS-6(D)	9.67	91.3	375.8	0.88	0.506	179.9
	WS-7-P(C)	8.00	81.7	286.0	0.99	0.705	110.9
	WS-8-P(D)	8.00	90.4	334.2	0.95	0.662	136.2
	WS-9(D)	9.67	74.7	294.9	1.08	0.568	89.4
	WS-10(D)	9.67	81.5	323.9	1.15	0.540	156.0
17	WS-12-N(D)	14.67	104.3	488.7	0.92	0.355	282.1
S	WS-13-N(D)	14.67	112.8	539.5	0.88	0.335	87.7
18	SB-1(D)	4.95	46.0	21.1	1.31	1.0	600.0
	SB-7(D)	4.95	46.0	21.3	1.26	1.0	460.0
U	SB-3(C)	7.00	62.0	90.1	1.27	0.977	356.2
	SB-9(B)	7.00	62.0	90.1	1.22	0.977	352.3
	*HB-40(B)	7.00	62.0	89.8	1.16	0.981	317.1
	SB-2(B)	8.25	66.0	80.3	1.09	0.759	279.6
	SB-8(C)	8.25	66.0	80.3	1.06	0.759	299.7
	*HB-41(B)	7.55	62.7	77.7	1.02	0.868	114.9
	SB-14(A)	5.00	72.4	127.2	0.96	0.864	68.6
	SB-4(A)	7.05	84.3	129.4	0.90	0.683	73.7
	SB-10(A)	7.05	76.9	123.9	0.99	0.728	87.4
	SB-5(A)	7.45	108.8	179.7	0.86	0.620	87.4
	SB-11(A)	7.45	83.6	165.0	0.93	0.752	75.4
	SB-6(A)	8.35	109.2	246.4	0.96	0.538	157.8

* = Composite steel-concrete section
U = Unsymmetrical steel section
S = Symmetrical steel section
(A) = 0% extrapolation
(B) = < 50% extrapolation
(C) = 50 to 100% extrapolation
(D) = > 100% extrapolation

sections (in negative bending). All specimens are normalized to 50,000 psi yield-strength steel. $M_{pe}-$ and the corresponding available inelastic rotation capacity, $\theta P-$, at $M_{pe}-$ are given for each specimen. $M_{pe}-$ is expressed as a percentage of the plastic moment, M_p-, in the table. Some of the test curves had to be extrapolated to determine the rotation capacity because the tests were not carried out far enough. The percent extrapolation is indicated for each specimen by a letter in parentheses after each specimen name in Table 2. The maximum moment reached in the test, M_{max}, is also given as a percentage of M_p-. Note that the guide specification slenderness limits do a reasonable job of ensuring that a compact section will at least reach M_p-. Specimen 188-3-6 is at the top of the table in boldface type. Because the actual yield point of the compression flange exceeded 50,000 psi and was greater than that of the web, $M_{pe}-$ was actually 97.4% of M_p- for this specimen. The rotation capacity at this level was 63.3 mrads vs. 58.0 mrads at M_p-. A rotation capacity of 63.3 mrads can therefore be considered as adequate for current plastic-design requirements.

The other 48 data points are plotted in Fig. 7. These data cover a range of b'/t from 5.0 to 14.7 and $2D_{cp}/t_w$ from 29.9 to 137.8. Except for one instance, the available rotation capacity at $M_{pe}-$ is greater than that provided by the AISC Part 2 section (188-3-6) with maximum slenderness ratios for the compression flange and web at M_p-. In the one situation, the rotation was 7% below that of the AISC Part 2 section. Because the plastic rotation requirement of 63.3 mrads can be regarded as an order-of-magnitude requirement, the procedure appears reasonable. Adequate rotation capacity is thus assured at $M_{pe}-$.

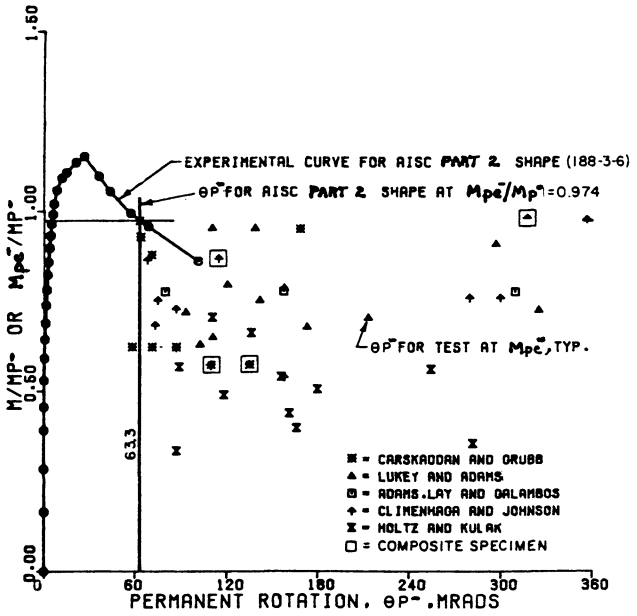

Fig. 7. Moment vs. permanent rotation test data

Overload

Research on the Autostress procedures started with a paper presented at the ASCE National Structural Engineering Meeting in San Francisco in April, 1973.[19] This paper suggested the classical shakedown theory be considered as a practical method of analysis of steel structures subjected to repeated loads. The shakedown analysis shows that permanent deformations caused by local yielding will eventually stabilize for independently variable loads below the shakedown limit.[20] After several loading cycles, the structure will behave elastically due to favorable residual stress patterns that are created by the local yielding. This theory seemed well-suited to the development of improved limit-state criteria for continuous bridges at overload.

Consider the deformed shape of the two-span continuous bridge in Fig. 8 after the dead load plus the AASHTO HS20 overload lane load has caused local yielding near the interior pier. In the absence of dead load or tie down, the permanent rotation resulting from the local yielding would cause the beam to lift off the center support. The self-equilibrating forces in Fig. 9 prevent this movement and create the indicated automoments. The autoforces and

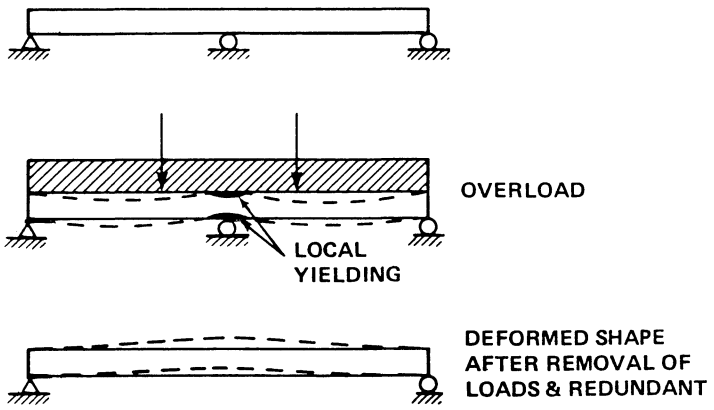

Fig. 8. Deformation caused by overloads

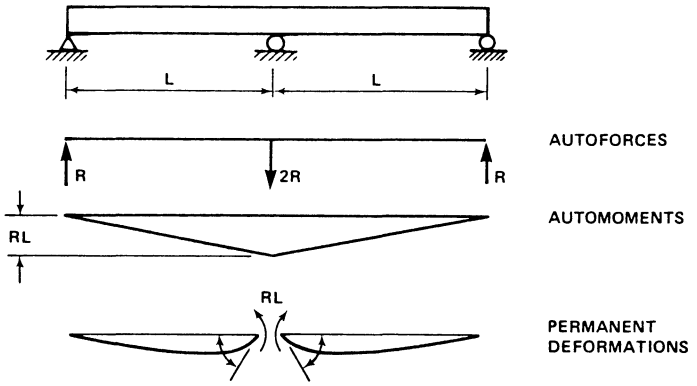

Fig. 9. Automoment diagram and permanent deformations

automoments are similar to the prestressing forces and moments in continuous beams only these forces and moments are created automatically as soon as the structure is subjected to heavy loads (no prestressing strands are used). These forces and moments coexist with the dead load in the structure after the live load is removed. The automoments ensure the structure remains elastic (or shakes down) when subjected to loads not exceeding the initial overload. They do not affect stress ranges related to fatigue design. A bridge member may never experience the automoments unless the actual loading is sufficiently heavy, which is acceptable. The permanent deformations caused by the automoments, including elastic and inelastic contributions, are shown in Fig. 9. They should be included in the dead-load camber to satisfy the Overload structural performance requirement.

The computation of the automoment for this structure is illustrated in Fig. 10. The computation is similar to that for AISC semirigid Type 3 building connections.[9,21] The interior-pier moment $M-$ is plotted vs. the permanent rotation at the pier $\theta P-$. Two curves are shown in Fig. 10. The first is an experimentally based moment-rotation curve for the pier section. The second is a straight line connecting Points A and B known as the beam line. Point A is the sum, M_e-, of the dead load MDL and overload live-load MLLE pier moments computed from an elastic analysis. $\theta P-$ is zero because Point A is based on elastic behavior. Point B is the total change in slope at the pier caused by the dead load and Overload live load assuming the pier to have a free hinge. This total rotation can be computed from simple elastic formulas using the same stiffness properties as used in computing Point A. Because Point B is based on a free hinge at the pier, the pier moment is zero. From superposition, any intermediate points fall on a straight line between Points A and B.

The actual overload pier moment MSH and permanent rotation are located at Point C, the intersection of the two curves. Point C can be determined graphically, or by writing equations for the two curves. MSH equals M_e- plus the pier automoment MAUTO. MAUTO is positive in this example, and effectively reduces MDL after the live load is removed. Thus, the maximum positive moment must be increased by the proper proportion of MAUTO before checking the total Overload stress in positive bending. Since the automoment remains in the structure, it is recommended that the composite moment of inertia, computed using a modular ratio of $3n$, be used to compute the stress in positive bending due to the automoment. No stress check is required at the interior pier. This is because no further permanent rotation occurs under subsequent applications of MLLE, as shown in Fig. 10. The automoments have caused the structure to shakedown. The permanent deflections due to the automoments can be computed from simple elastic deflection formulas (using the $3n$ moment of inertia) and included in the camber.

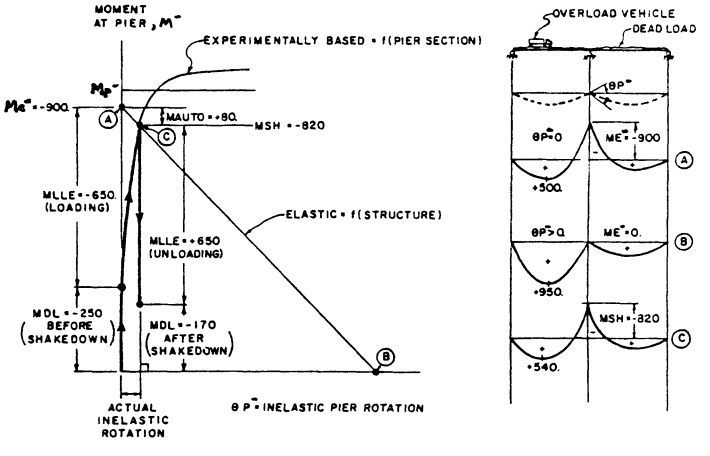

Fig. 10. Graphic determination of automoment and permanent rotation

The above computations assume there is no yielding in positive bending. Yielding in positive bending increases the permanent rotation at the pier. Ref. 22 describes procedures to adjust the beam line for positive-moment yielding. Also, when a bridge is continuous over more than one interior pier, carry-over of automoments occurs. The automoment at one pier influences the dead-load moments at the other piers. An iterative solution is then required.

In the absence of experimentally based moment-rotation curves for the pier sections, two experimentally determined curves are given in the guide specification for computing automoments at overload. The dashed curve in Fig. 11 is for an unsymmetrical welded all-steel section from Ref. 12 (Specimen 188-3-2) with a cover plate on one flange to simulate the composite rebars. It was determined from examining the available moment-rotation test data that all-steel specimens have sufficiently similar behavior at low plastic rotations to permit the use of a single curve. This curve should be used for non-composite beams, and to determine any automoments and respective camber requirements due to non-composite dead load on composite beams. The maximum stress in positive bending due to elastic non-composite moments plus any corresponding automoments is limited to $0.80*F_y$.

The dotted curve in Fig. 11 is for an actual composite specimen from Ref. 13 (Specimen 188-3-4W) with the same steel section as Specimen 188-3-2 without the cover plate. The specimen was from a half-scale interior-support model of a composite steel-concrete section subjected to negative bending. The permanent rotations are larger for the composite specimen 188-3-4W probably because of concrete cracking. Also, because the concrete slab shifted the plastic neutral axis more than the cover plate, Specimen 188-3-4W was not able to reach as high a moment. Thus, the solid curve is the curve for Specimen 188-3-4W shifted vertically to reach M_p- at the same $\theta P-$ value as Specimen 188-3-2. Beyond that value of $\theta P-$, no increase in moment is conservatively assumed. This solid curve should be used to determine the automoments and required camber due to

the composite dead load and overload live load on composite beams. For this calculation, it is recommended that the origin of the axes be shifted so that it starts on the solid curve at the non-composite dead-load moment. Note the curves are normalized with respect to M_p- in Fig. 11. Therefore, the pier section must meet the compact-section requirements in Eqs. 3–7 to use these curves.

The permanent pier rotation at overload is assumed to be

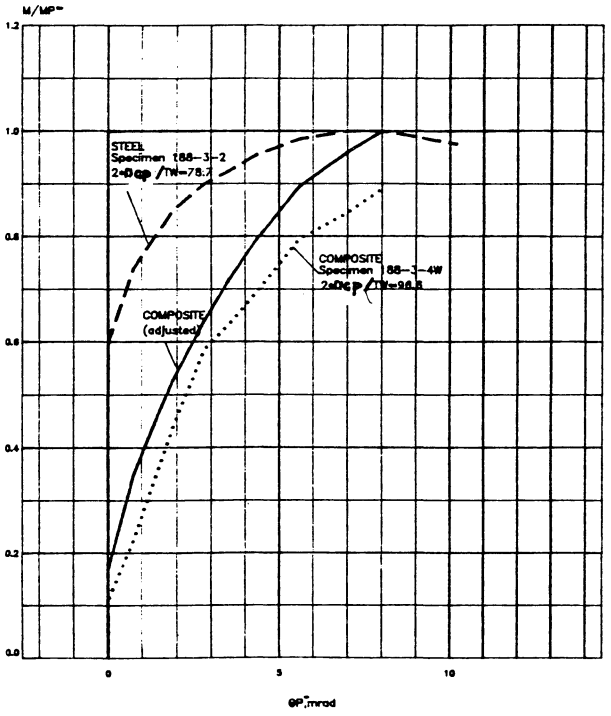

Fig. 11. Guide specification moment vs. permanent rotation curves-overload

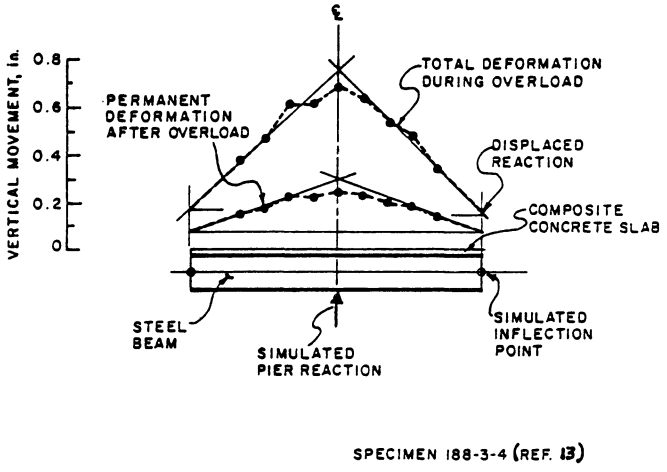

Fig. 12. Roadway profile during and after overload

concentrated at the pier, which would be similar to the angle change at a pier with two true simple supports. However, the model test in Ref. 13 indicated the permanent rotation at overload is actually smoothly distributed across the interior-pier reaction, shown in Fig. 12, because rebars remained elastic. Most of the yielding occurs in the compression region of the steel section because of the shift in the neutral axis due to the composite rebars. The rebars can probably be considered elastic at overload, as required by the guide specification, if the steel section F_y does not exceed 50,000 psi and the rebar F_y is not below 60,000 psi.

CONCLUSIONS AND FUTURE WORK

The improved limit-state criteria presented in the AASHTO guide specification for braced compact sections have resulted in demonstrated economies in short-span steel bridge designs. The criteria were applied in the design of the Whitechuck River Bridge, which proved to be cost competitive with other methods of construction. This bridge on a National Forest Service logging road was instrumented and tested under heavy loads and showed no signs of distress during or after the tests.[7] A design example has been prepared to accompany the guide specification which shows how a W36 rolled beam (without cover plates) can be used on a 100-ft span in a two-span continuous-beam highway bridge.[23] A rolled-beam bridge has also been designed by the New York State DOT using the guide specification.

Research on extending the improved limit-state criteria to plate girders is presently underway. Initial moment-rotation tests on plate girders in negative bending have been conducted, and sample designs are being prepared for examination as a continuation of AISI Project 188.[8] Composite plate girders in positive bending are being tested in AISI Project 320A.[24] A research project is also ongoing at the new FHWA Turner-Fairbank Structural Laboratory as part of AISI Project 330. Tests will be conducted on a 0.4 scale model of a two-span, three-girder bridge with precast post-tensioned deck panels. The plate-girder bridge was designed using the Autostress procedures. A component test of the negative-moment region of one of the bridge girders has recently been completed.

ACKNOWLEDGMENTS

The development of the Autostress procedures was a team effort at the U.S. Steel Technical Center in Monroeville, Pa. The author gratefully acknowledges the efforts of Dr. Geerhard Haaijer, vice president and director of engineering for AISC, and Phillip S. Carskaddan of AISC Marketing, Inc., who were responsible for the initial development of the Autostress procedures. The guide specification was prepared by Dr. Haaijer. The project was sponsored by AISI. The AISI staff representative is Albert C. Kuentz. Many thanks for the advice from the members of the AISI

Autostress Advisory Task Force, and to the many people involved in the design, construction and testing of the Whitechuck River bridge.

REFERENCES

1. *Association of State Highway and Transportation* Standard Specifications for Highway Bridges *13th Ed., 1983.*
2. *Haaijer, G., C. G. Schilling and P. S. Carskaddan* Limit-State Criteria for Load-Factor Design of Steel Bridges *Engineering Structures. Butterworth and Co. Ltd., Vol. 5, No. 1, January 1983, Surrey, England (pp. 26–30).*
3. *American Association of State Highway and Transportation Officials* Guide Specification for Alternate Load-Factor Design Procedures for Steel Beam Bridges Using Braced Compact Sections *Draft Copy, Aug. 28, 1985.*
4. *Haaijer, G., P. S. Carskaddan and M. A. Grubb* Autostress Design of Steel Bridges *ASCE Journal of Structural Engineering, Vol. 109, No. ST1, January 1983 (pp. 188–199).*
5. *Haaijer, G., P. S. Carskaddan and M. A. Grubb* Suggested Autostress Procedures for Load Factor Design of Steel Beam Bridges *American Iron and Steel Institute, Project 188, March 1, 1985, Washington, D.C.*
6. *American Institute of Steel Construction, Inc.* Proposed Load and Resistance Factor Design Specification for Structural Steel Buildings *Sept. 1, 1983, Chicago, Ill.*
7. *Roeder, C. W. and L. Eltvik* Autostress Design Criteria—Load Test of the Whitechuck River Bridge *FHWA Project DTFH61-81-C-00114, University of Washington, January 1985, Seattle, Wash.*
8. *Schilling, C. G.* Moment-Rotation Tests of Steel Bridge Girders *American Iron and Steel Institute, Project 188, April 15, 1985, Washington, D.C.*
9. *American Institute of Steel Construction, Inc.* Specification for the Design, Fabrication, and Erection of Structural Steel for Buildings *8th Ed., 1980, Chicago, Ill.*
10. *Carskaddan, P. S., G. Haaijer and M. A. Grubb* Computing the Effective Plastic Moment *AISC Engineering Journal, 1st Qtr., 1982, Chicago, Ill. (pp. 12–15).*
11. *Grubb, M. A. and P. S. Carskaddan* Autostress Design of Highway Bridges, Phase 3: Moment-Rotation Requirements *American Iron and Steel Institute, Project 188, July 6, 1981, Washington, D.C.*
12. *Grubb, M. A. and P. S. Carskaddan* Autostress Design of Highway Bridges, Phase 3: Initial Moment-Rotation Tests *American Iron and Steel Institute, Project 188, April 18, 1979, Washington, D.C.*
13. *Carskaddan, P. S.* Autostress Design of Highway Bridges, Phase 3: Interior-Support-Model Test *American Iron and Steel Institute, Project 188, Feb. 11, 1980, Washington, D.C.*
14. *Adams, P. F., M. G. Lay and T. V. Galambos* Experiments on High-Strength Steel Members *Fritz Engineering Laboratory Report No. 297.8, Lehigh University, July 1984, Bethlehem, Pa.*
15. *Lukey, A. F. and P. F. Adams* Rotation Capacity of Beams Under Moment Gradient *ASCE Journal of Structural Engineering, June 1969.*
16. *Holtz, N. M. and G. L. Kulak* Web Slenderness Limits for Compact Beams *Structural Engineering Report No. 43, University of Alberta, March 1973.*
17. *Holtz, N. M. and G. L. Kulak* Web Slenderness Limits for Non-Compact Beams *Structural Engineering Report No. 51, University of Alberta, August 1975.*
18. *Climenhaga, J. J. and R. P. Johnson* Local Buckling in Continuous Composite Beams *The Structural Engineer, September 1972.*
19. *Haaijer, G.* Autostress Design of Steel Structures *ASCE National Structural Engineering Meeting, Preprint No. 1930, April 9–13, 1973, San Francisco, Cal.*
20. *American Society of Civil Engineers* Commentary on Plastic Design in Steel *Manual of Engineering Practice 41, 1971 (pp. 106–116).*
21. *Disque, R. O.* Wind Connections with Simple Framing *AISC Engineering Journal, Vol. 1, No. 3, July 1964, Chicago, Ill. (pp. 101–103).*
22. *Carskaddan, P. S., G. Haaijer and M. A. Grubb* Adjusting the Beam-Line Method for Positive-Moment Yielding *AISC Engineering Journal, Vol. 21, No. 4, Chicago, Ill (pp. 217–221).*
23. *Grubb, M. A.* Design Example—Two-Span Continuous Beam Highway Bridge Designed by the Autostress Method *American Iron and Steel Institute, Project 188, May 10, 1985, Washington, D.C.*
24. *Vasseghi, A. and K. H. Frank* Ultimate Strength of Composite Steel Plate Girders—AISI Project 320—Test Results of Girder 1 *Phil M. Ferguson Structural Engineering Laboratory Report, University of Texas, August 1984, Austin, Texas.*